Catalysis Science & Technology

PAPER

View Article Online
View Journal | View Issue

Cite this: *Catal. Sci. Technol.*, 2019, **9**, 2152

Lean and rich aging of a Cu/SSZ-13 catalyst for combined lean NO_x trap (LNT) and selective catalytic reduction (SCR) concept

Xavier Auvray,[a] Ann Grant,[b] Björn Lundberg[b] and Louise Olsson *[a]

In the combined lean NO_x trap (LNT) and selective catalytic reduction (SCR) concept, the SCR catalyst can be exposed to rich conditions during deSO_x of the LNT. Aging of Cu/SSZ-13 SCR catalysts, deposited on a cordierite monolith, was therefore studied in rich, lean and cycling lean/rich operations at 800 °C (lean condition: 500 ppm NO, 8% O_2, 10% H_2O and 10% CO_2; rich condition: 500 ppm NO, 1% H_2, 10% H_2O and 10% CO_2). The structure of the catalyst was investigated by X-ray diffraction (XRD), surface area measurements and scanning transmission electron microscopy (STEM). In general, aging decreased the SCR activity and NH_3 oxidation. However, rich conditions showed a very rapid and intense deactivation, while lean aging led to only a small low-temperature activity decrease. The XRD results showed no sign of structure collapse, but the number of active sites, as titrated by NH_3 temperature-programed desorption (NH_3-TPD) and *in situ* DRIFTS, revealed an important loss of acid sites. NH_3 storage was significantly more depleted after rich aging than after lean aging. The Lewis sites, corresponding to exchange Cu^{2+}, were preserved to some extent in lean conditions. Lean aging also decreased the enthalpy of NH_3 adsorption from −158 kJ mol^{-1} to −136 kJ mol^{-1}. Moreover, a comparison of aging in lean-rich cycling conditions with aging only in rich conditions revealed that adding lean events did not hinder or reverse the deactivation, and it was mainly the time in rich conditions that determined the extent of the deactivation. The STEM images coupled with elemental analysis revealed the formation of large Cu particles during rich aging. Conversely, Cu remained well dispersed after lean aging. These results suggest that the copper migration and agglomeration in large extra-framework particles, accelerated by the action of hydrogen, caused the observed severe deactivation.

Received 21st December 2018,
Accepted 17th March 2019

DOI: 10.1039/c8cy02572j

rsc.li/catalysis

Introduction

Emissions of nitrogen oxides (NO_x) are a growing problem and a major concern for air quality in urban areas. An important source of these emissions is the transportation sector. To reduce NO_x emissions from diesel vehicles, two catalytic systems have been developed in parallel. The first, the lean NO_x trap (LNT) stores NO_x on a catalyst containing a storage component, such as Ba, during lean operation of the engine, *i.e.* in a large excess of oxygen. Periodically, when the catalyst approaches saturation and its trapping efficiency decreases, the engine operates in rich conditions to provide reductants (hydrocarbons and CO) to the exhaust gas, which reduce the stored NO_x into N_2. Thus, the catalyst is purged and the trapping process in lean conditions can be reiterated. This system has the advantage of being able to store efficiently NO_x at quite low temperature, but it is sensitive to sulfur compounds that form stable sulfate on the NO_x storage component, impeding the NO_x-trapping ability and thus requiring regular desulfurization (deSO_x). Indeed, after sulfur exposure, an LNT can be regenerated at high temperature and in rich conditions.[1] The second NO_x removal strategy is to continuously dose in the exhaust a compound that selectively and efficiently reduces the NO_x in the presence of an excess of oxygen, such as NH_3 for selective catalytic reduction (SCR). Although SCR enables full NO_x reduction at some temperatures, it cannot be used below *ca.* 200 °C because urea cannot be dosed at low temperature without major issues with deposits.

The combination of a NO_x-trap catalyst and an SCR system can, however, be used to broaden the temperature interval. In this regard, dual catalysts and the passive SCR of stored NO_x have been studied.[2–6] Research has confirmed that the presence of an SCR catalyst downstream of an LNT improves the NO_x conversion and suppresses the NH_3 slip during LNT purge.[7,8] However, this configuration implies the exposure of the SCR catalyst to high temperature during LNT regeneration and desulfurization, which can modify the SCR catalyst and impair its efficiency. Regeneration of the upstream

[a] *Competence Centre for Catalysis (KCK), Chemical Engineering, Chalmers University of Technology, SE-412 96 Göteborg, Sweden. E-mail: louise.olsson@chalmers.se*
[b] *Volvo Car Corporation, SE-405 31 Göteborg, Sweden*

particulate filter can also lead to a high temperature exhaust and oxygen depletion.[9] The effects of hydrothermal aging,[10–16] sulfur exposition and regeneration[17–19] have been studied to better understand the aging mechanism under practical operating conditions. Collapse of the zeolite structure, active metal agglomeration and dealumination are the most common identified aging mechanisms that occur during thermal aging.[14] It seems clear that small pore zeolites, with the chabazite structure, are more resistant against hydrothermal deactivation than the more widely studied large- and medium-pore-size zeolites, such as beta, ZSM-5 and Y.[7,11,15] It has been proposed that a small pore size hinders the dealumination mechanism, which consists of the extraction and migration of the framework aluminium.[15] $Al(OH)_3$ has been proposed to be the intermediate moiety formed, thereby causing dealumination.[20,21] Fickel *et al.* calculated that $Al(OH)_3$ would be too large to exit the cage of the CHA zeolite structure.[20] The role of Cu in promoting the structure collapse has also been evidenced[10,15,20] and here, copper aluminate is also considered as an intermediate.[15,21] Several authors have noted that a high Cu loading and high Si/Al diminish the resistance to the hydrothermal aging of Cu/SSZ-13[10,22,23] due to the higher proportion of Cu exchanged on CHA cage sites, which are less stable and more prone to agglomeration than the species bound to 6-membered ring locations.[21,24] In 2008, Huang *et al.*[9] studied the effects of a low concentration of oxygen and of various reductants (H_2, CO and C_3H_6) on a commercial Cu/zeolite catalyst aged at 650 °C. While CO had no impact and C_3H_6 caused reversible SCR deactivation due to blocking of the sites, exposure to H_2 in combination with the low oxygen concentration led to significant and irreversible deactivation.

However, to the best of our knowledge, there are no studies available in the literature investigating the aging of the Cu/CHA SCR catalyst during rich regeneration of the NO_x storage catalyst. Further, the impact of alternating between lean and rich conditions on the Cu/SSZ-13 morphology and activity should be addressed. In the present work, the impact of rich, lean and lean/rich cycling aging on a monolithic Cu-exchanged SSZ-13 catalyst was evaluated. Standard SCR with NH_3 as well as NH_3 oxidation were performed and the activity evolution after aging was studied. The aging temperature was set at a constant of 800 °C but the aging duration was varied to allow relevant comparisons. The catalysts were characterized by X-ray diffraction (XRD), scanning transmission electron microscopy (STEM) and energy dispersive X-ray spectroscopy (EDX) mapping. NH_3 adsorption was studied by NH_3-TPD and differential scanning calorimetry (DSC).

Experimental methods

Chabazite zeolite synthesis

The chabazite zeolite SSZ-13 was synthesized by hydrothermal conversion of a faujasite-type zeolite, according to a procedure reported by Zones *et al.*[25] First, a solution of NaOH (1 M) was prepared by dissolving NaOH pellets (Sigma Aldrich, >98% anhydrous pellets) into deionized water (Millipore). Then, 250 g of sodium trisilicate (Na_2SiO_3, VWR) and 320 g of deionized water were then poured into 200 mL of the prepared NaOH solution under stirring. After 15 min stirring, 25 g of zeolite Y (Zeolyst, CBV720) was added to the solution and the mixture stirred for 30 min at room temperature. Finally, 105 g of the structure-directing agent (SDA) *N*,*N*,*N*-trimethyl-1-adamantanamine iodide (TMAAI, ZeoGen SDA 2825) was added to the solution. The mixture was kept under stirring for another 30 min before being transferred to the Teflon cup of a Parr stainless steel autoclave. The hydrothermal aging was carried out in autoclaves, filled up to 2/3 of their volume, at 140 °C in an oven for 6 days without mechanical stirring. The solid fraction was recovered by centrifugation and washed with deionized water until the pH of the washing solution became neutral (6–7 times). The powder was then dried for at least 12 h at room temperature and calcined for 8 h at 550 °C with a heating rate of 0.5 °C min^{-1}. The sodium form of the zeolite (Na/SSZ-13) was thus obtained.

Ion exchange of SSZ-13

Two ammonium exchanges were performed prior to the Cu ion exchange. A solution of ammonium nitrate (2.0 M) was prepared by dissolving NH_4NO_3 (Sigma-Aldrich ≥99.0%) in deionized water. The zeolite powder was poured into a volume of ammonium nitrate solution corresponding to 33.33 mL g^{-1} of zeolite. The mixture was stirred and heated up in an oil bath at 80 °C for 15 h. The powder collected was washed until the pH became neutral and was then dried for 12 h. Then, the ammonium exchange operation was repeated a second time. The Cu exchange was performed by mixing the obtained zeolite with a solution of copper nitrate (0.2 M) with the same solution-to-catalyst ratio as the ammonium exchange (100 mL/3 g). The mixture was maintained in an oil bath at 80 °C for 2 h under vigorous stirring. The copper nitrate solution was prepared by dissolving copper nitrate hemi(penta-hydrate) ($CuN_2O_6{\cdot}2.5H_2O$, Sigma-Aldrich) into deionized water. After washing and subsequent drying for at least 12 h, the zeolite was calcined for 4 h at 550 °C (5 °C min^{-1} heating rate).

Monolith preparation

The samples tested in flow reactor consisted of catalyst powder coated on a commercial cordierite honeycomb monolith, the channel density of which was 400 cpsi. The monolith dimensions were: length = 20 mm, diameter = 20 mm. The washcoat was composed of 5 wt% of boehmite (Disperal P2, Sasol) and 95 wt% of the prepared Cu-exchanged zeolite. This blended powder was then dispersed in an aqueous solution of ethanol (50 wt% of milliQ water + 50 wt% of ethanol of spectroscopic purity grade, (Merck)). The slurry had a liquid-to-solid weight ratio of 4 and was kept under stirring. The dip-coating method was used to deposit the washcoat on the

bare monolith, which had previously been calcined (2 h at 600 °C with 1 h ramping) to remove any possible impurity. After immersion of the monolith, it was slowly dried under an air stream (≈60 °C) while being flipped and rotated to allow homogeneous wetting and deposition on all the inner walls. The monoliths were further dried under a hot air stream (600 °C) for 1 min until all the channels were free of liquid. The procedure was repeated until the mass of washcoat was around 700 mg. Finally, the samples were calcined in air at 500 °C for 2 h.

Activity test and aging

Activity measurements and aging were carried out on the monolithic samples placed in a quartz tube horizontal reactor, the inner diameter of which was 22 mm. A resistance, coiled around the tube and connected to a Eurotherm controller, provided for controlled heating. Two K-type thermocouples were inserted by the reactor rear end to monitor the temperature inside the monolith and of the inlet gas, 2–2.5 cm in front of the sample. The gases were supplied by a set of mass flow controllers (Bronkhorst) and the effluent gas was analyzed by FTIR spectroscopy (Multigas2030, MKS). The fresh sample was first de-greened for 3 h at 600 °C under standard SCR conditions (500 ppm NO, 500 ppm NH_3, 8% O_2, 5% H_2O in argon) with a total flow of 3.5 L min^{-1}, corresponding to a GHSV of 33 423 h^{-1}. NH_3-TPD, standard SCR and NH_3 oxidation measurements were all preceded by a 20 min oxidation step at 500 °C (8% O_2), performed with a total flowrate of 3.5 L min^{-1}. The gas compositions were always balanced by Ar.

For NH_3-TPD, NH_3 adsorption was carried out at 200 °C, in order to avoid the weak physisorption of NH_3 (500 ppm NH_3, 5% H_2O, 40 min). The catalyst was flushed in Ar for 40 min before the temperature was increased (10 °C min^{-1}) up to 600 °C, to release the adsorbed NH_3.

Steady-state NH_3 conversion was measured for NH_3 oxidation at temperatures ranging between 250 °C and 500 °C. The gas composition used was 500 ppm NH_3, 8% O_2 and 5% H_2O.

Standard SCR was carried out in the same manner with a wider temperature range (125–500 °C) and using a feed gas containing 500 ppm NO, 500 ppm NH_3, 8% O_2 and 5% H_2O.

Aging was carried out in the same reactor at 800 °C during a variable time. Samples were aged in rich conditions, lean conditions and in cycling between lean and rich conditions, respectively. The latter case was used since the LNT system was operated with lean and rich phases. Two lean/rich aging procedures were studied with the same lean/rich time ratio of 15 to evaluate the effect of cycling frequency. The lean/rich aging denoted "long" consisted of lean periods of 15 min and rich pulses of 1 min. The lean/rich aging denoted "short" had 5 min lean periods and rich pulses lasting 20s. The lean gas feed was composed of 500 ppm NO, 8% O_2, 10% H_2O and 10% CO_2. The rich gas composition was 500 ppm NO, 1% H_2, 10% H_2O and 10% CO_2.

Catalyst characterization

The crystalline structure of the zeolite was studied by X-ray diffraction with a Siemens diffractometer D5000 operating at 40 kV, using the Kα_1 emission ray of a Cu anode as the X-ray source (λ = 1.54060 Å). The aged samples were crushed monoliths, including the cordierite support, while the fresh sample was pure Cu/SSZ-13.

The elemental composition of the fresh catalyst was determined by ICP-AES (ALS Scandinavia). This revealed that the Si/Al ratio of the prepared catalyst was 18 and the Cu content was 1.63 wt%.

The specific surface area was measured according to the BET method on a Micromeritics Tri-Star 3000. The samples were degassed at 250 °C for 5 h under a N_2 flow. The specific surface area measured for pure cordierite was 0.7 m^2 g^{-1}, which is negligible. The BET surface area of the Cu/SSZ-13 catalysts was calculated from the area measured on the crushed monoliths and the catalyst loading of each monolith.

The shape and composition of the catalyst particles were examined using STEM-EDX. Powder was scraped off the aged monoliths and the fresh sample powder was degreened in the flow reactor. The resulting powder was subsequently put on holey carbon films on TEM Cu grids. The particles were imaged using an FEI Titan 80–300 TEM with a probe Cs (spherical aberration) corrector operated at 300 kV. The images were recorded using a high-angle annular dark field (HAADF) detector in the scanning TEM imaging mode (STEM), providing *Z* number contrast.

DRIFT spectroscopy of NH_3 adsorption

NH_3 adsorption was conducted on powder samples, which were placed in the cup of a heated Praying Mantis DRIFT cell (Harrick Scientific) equipped with KBr windows and mounted on a Vertex 70 FTIR spectrometer (Bruker) equipped with a liquid N_2-cooled MCT detector. The spectra were recorded with a resolution of 1 cm^{-1}. Fresh Cu/SSZ-13 powder was pretreated in a ceramic crucible, placed in the flow reactor previously described, according to the degreening procedure. This sample was referred to as degreened. Aged samples, as for the XRD analysis, were obtained by crushing the aged monoliths, which resulted in them containing cordierite. Prior to NH_3 adsorption, the samples were dehydrated at 500 °C for 30 min in 8% O_2 in Ar. Cooling to 150 °C was carried out in an Ar flow. After 30 min, a spectrum was recorded (24 scans), which was used as the background. Then, 1000 ppm NH_3 was flowed through the catalyst bed at 150 °C. After 20 min of NH_3 adsorption, the samples were flushed with Ar for 60 min. The spectra (accumulation of 16 scans) were recorded every 5 min during the NH_3 adsorption and subsequent Ar exposure. The gas flow rate during the whole procedure was constant (50 mL min^{-1}).

Micro-calorimetry experiments

NH_3 adsorption and TPD were performed in a differential scanning calorimeter set-up (Sensys, Setaram) connected to a

mass spectrometer (Hiden Analytical) on the fresh and aged catalysts. Two quartz tubes equipped with a sintered quartz bed were mounted vertically in the instrument. The reference tube was left empty during the experiments. The aged samples consisted of washcoat scraped off aged monoliths, whereas the fresh sample was as-prepared Cu/SSZ-13 and needed to be de-greened in the calorimeter before measurements. Here, *ca.* 20 mg of powder was placed in the sample tube of the calorimeter and the total flow used was 20 mL min^{-1}. The concentration of NH_3 was 500 ppm and NH_3 adsorption was performed at 200 °C. After flushing with argon for 1 h, the temperature was ramped up at a rate of 10 °C min^{-1} to 600 °C to carry out the NH_3 desorption.

Results and discussion

Characterization of fresh Cu/SSZ-13

X-ray diffraction was performed on the fresh catalyst powder to check that the desired crystalline structure, SSZ-13, was obtained by the synthesis method employed. The peak positions confirmed that the obtained zeolite had the SSZ-13 structure and good crystallinity. The diffractograms obtained for the aged samples showed peaks corresponding to both the cordierite support and zeolite washcoat (due to the crushed monoliths used). They indicated that the zeolite structure was preserved during aging at 800 °C, even after a 32 h treatment (Fig. 1 (L/R 32 h)). However, as demonstrated by Blakeman *et al.*,[15] the zeolite structure can be lost at high temperature and restored after cooling. The presence of cordierite, in a high content, in the aged samples has a dilution effect and decreased the peak intensity corresponding to the zeolite catalyst. Therefore, a physical mixture of fresh catalyst powder and crushed cordierite of a similar composition as the monolithic samples was prepared and analyzed for better comparison of the diffractograms. No diffraction peak corresponding to Cu or CuO crystallites were observed ($2\theta_{Cu(111)}$ = 43.6°, $2\theta_{CuO(111)}$ = 38°,), indicating the high Cu dispersion, even after aging, which is in agreement with previous reported XRD results.[7,14]

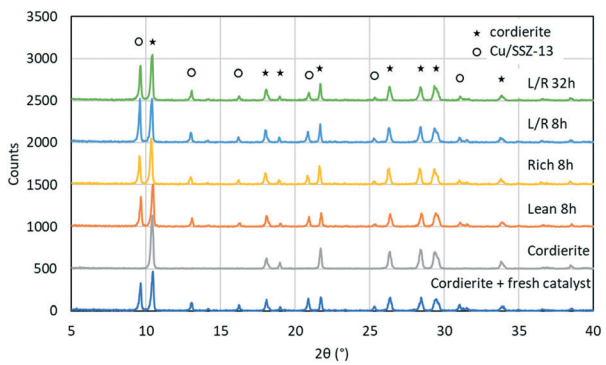

Fig. 1 X-ray diffractogram of a mixture of fresh Cu/SSZ-13 (25 wt%) + cordierite (75 wt%), pure cordierite and crushed monolithic samples after aging for 8 h in lean (lean 8 h), 8 h in rich (rich 8 h), 8 h in cycling conditions between lean (15 min) and rich (1 min) (L/R 8 h) and 32 h in cycling conditions between lean (15 min) and rich (1 min) (L/R 32 h).

Unlike the structure and crystallinity, the specific surface area, as calculated from N_2 adsorption according to the BET method, was impacted by aging. The calculations took into account the 75 wt% of cordierite and that the cordierite specific surface could be neglected. As shown in Table 1, lean aging greatly decreased the surface area of the zeolite, *i.e.* from 737 m^2 g^{-1} to 534 m^2 g^{-1}. Rich conditions had a milder effect on the surface area and, consequently, the sample aged in L/R cycling conditions had a higher surface area than the lean-aged one. This surface area decrease seems in contradiction with the XRD but it indicates that even though the long-range order and structure of the zeolite was preserved, local pore collapse and pore blockage happened to some extent during aging. It is therefore not surprising that a lower BET surface area was measured for the sample aged the longest (32 h).

Standard SCR

Activity for standard SCR was measured over monolithic catalysts at temperatures ranging from 125 °C to 500 °C, before and after aging. The results are presented in Fig. 2 and 3, which are divided in to two subplots representing NH_3 conversion (a) and NO conversion (b), respectively. All the samples strictly showed the same activity at all temperatures after degreening; therefore, only one curve was included in the figures as the reference. Fig. 2 compares the activity after aging for 8 h in several conditions: lean (500 ppm NO, 8% O_2, 10% H_2O and 10% CO_2), rich (500 ppm NO, 1% H_2, 10% H_2O and 10% CO_2) and cycling between lean and rich conditions (long and short periods), while Fig. 3 compares the effect of rich aging for 2 and 8 h, respectively, as well as aging in cycling conditions for 32 h. NH_3 conversion (Fig. 2a and 3a) showed a sharp increase from near null at 125 °C up to 100% at 250 °C for the degreened catalyst. After lean aging, the catalyst was mainly deactivated at temperatures below 250 °C and did not reach 100% conversion. Two samples were aged in cycling conditions between lean and rich with the same lean/rich time ratio but different period durations, *i.e.* 15 min lean per 1 min rich for the denoted "L/R long" aging and 5 min lean per 20 s rich for the "L/R short" aging. Keeping the lean/rich time ratio and the total aging time (8 h) constant led both samples to experience the same exposure time to lean and rich conditions, respectively. Thus, the effect of the switching frequency can be inferred. It appears that this

Table 1 BET surface area of fresh and aged samples

Samples	BET surface area (m^2 g^{-1})
Cu/SSZ-13 fresh	737
Lean 8 h	534
Rich 8 h	612
Lean-rich long 8 h	595
Lean-rich long 32 h	436
Rich 2 h	597

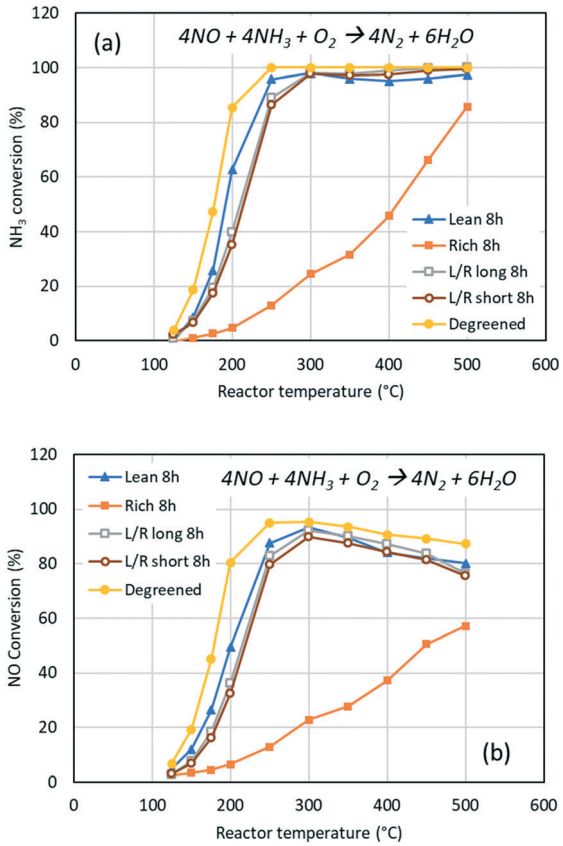

Fig. 2 Standard SCR activity of degreened and aged Cu/SSZ-13 catalysts. (a) NH_3 conversion and (b) NO conversion (500 ppm NO, 500 ppm NH_3, 8% O_2, 5% H_2O in Ar. Total flow = 3.5 L min^{-1}). Aging at 800 °C using lean conditions: 500 ppm NO, 8% O_2, 10% H_2O and 10% CO_2 and rich conditions: 500 ppm NO, 1% H_2, 10% H_2O and 10% CO_2.

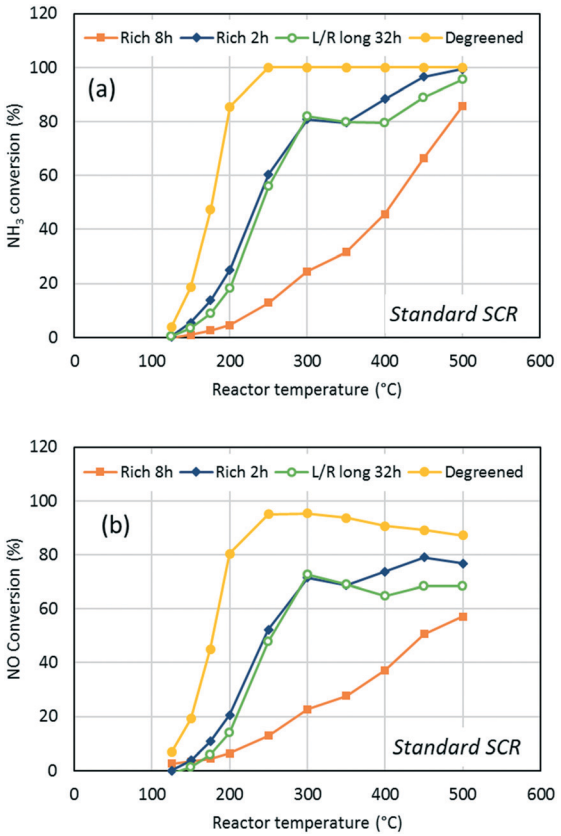

Fig. 3 Standard SCR activity of degreened and aged Cu/SSZ-13 catalysts. (a) NH_3 conversion and (b) NO conversion (500 ppm NO, 500 ppm NH_3, 8% O_2, 5% H_2O in Ar. Total flow = 3.5 L min^{-1}). Aging at 800 °C using lean conditions: 500 ppm NO, 8% O_2, 10% H_2O and 10% CO_2 and rich conditions: 500 ppm NO, 1% H_2, 10% H_2O and 10% CO_2.

parameter did not significantly affect the resulting activity since both samples showed similar SCR activity (Fig. 2a and b). The deactivation after 8 h cycling aging was more pronounced than after 8 h lean aging, especially for NH_3 conversion below 250 °C. For example, at 200 °C, the activity dropped from over 80% to less than 40%. Finally, the 8 h rich aging led to a tremendously lower SCR activity over the whole temperature range. The highest NO_x conversion was observed at 500 °C and remained below 60% (Fig. 2b).

It should be noted that NH_3 conversion (Fig. 2a) was consistently higher than NO conversion (Fig. 2b) for both the degreened and aged catalysts due to NH_3 consumption in the side-reactions, typically NH_3 oxidation into N_2. As the latter reaction proceeds to a larger extent at high temperature, NO conversion decreased with temperature after reaching a maximum around 300 °C. Meanwhile NH_3 conversion remained constant near 100%. Only in the case of the rich aging did NO conversion increase continuously with temperature due to the overall lower conversion. Contrary to other Cu-exchanged zeolites, such as BEA and Y,[11,26] Cu/SSZ-13 usually exhibits a high N_2 selectivity and little N_2O production in standard SCR tests, which was also the case for our catalyst. Less than 5 ppm N_2O was produced by the fresh samples at the highest amount. This amount increased after aging (<10 ppm), except after aging in rich conditions (2 h and 8 h).

Fig. 3 emphasizes the outstanding effect of aging in rich conditions as the deactivation was already strong after 2 h aging, as depicted by the high light-off temperature and the temperature of full ammonia conversion (500 °C). The results obtained after 2 h rich aging and 32 h lean/rich aging revealed the occurrence of two SCR mechanisms, which had different temperature windows, *i.e.* "high" and "low" temperature SCR mechanisms. This was evidenced by the activity decline between 300 °C and 350 °C for the 2 h rich aged and between 300 °C and 400 °C for the 32 h lean/rich aged sample, respectively. This decrease resulted from the concomitant decline of the low-temperature SCR mechanism and the low rate of the high-temperature mechanism over a narrow temperature window. Such non-monotonic SCR activity profiles were also observed by Ma *et al.*[27] A low and high temperature mechanism was proposed by Paolucci *et al.*[28] using a combination of experiments and *ab initio* calculations. At low temperature, the active copper forms copper-pairs that are solvolysed by ammonia. However, this is not the case at higher temperature. Moreover, earlier kinetic modelling of Cu/SSZ-13 also suggested a low and high temperature mechanism for ammonia SCR.[29]

Since the 2 h rich and 32 h lean/rich aged catalysts exhibited similar activity below 300 °C, it suggested that the rich conditions control the aging process, resulting in low activity within this temperature interval. The 32 h aging in the cycling conditions was designed to comprise a total rich time of 2 h to allow comparison with the 2 h rich aging. It was remarkable that the additional 30 h aging in lean conditions had no additional effect on the SCR activity below 300 °C. This also means that the effect of rich exposure was irreversible and could not be mitigated by regularly switching to lean conditions. We suggest that rich conditions strongly affect the low-temperature mechanism, while lean conditions have a more reasonable impact. However, the two catalysts behaved differently above 300 °C where the 32 h aged catalyst showed lower activity, which indicated that the additional long exposure at 800 °C in lean conditions had an impact on the high-temperature mechanism.

NH_3 oxidation

As seen in Fig. 2 and 3, NH_3 oxidation plays a role during SCR as it consumes NH_3 and limits the conversion of nitric oxide. It is therefore interesting to measure the catalyst ability to oxidize NH_3 in the absence of NO and, more importantly, the effect of various aging conditions on NH_3 oxidation. Fig. 4 shows the degreened and aged activity profiles of the lean-aged (500 ppm NO, 8% O_2, 10% H_2O and 10% CO_2) and the rich-aged (500 ppm NO, 1% H_2, 10% H_2O and 10% CO_2) samples. NH_3 conversion remained below 30% up to 400 °C and then lit off to reach 100% at 500 °C. Both lean and rich aging impaired the activity, as evidenced by the conversion below 20% up to 450 °C. Over this temperature range, the rich-aged catalyst showed lower activity. However, at 500 °C, its activity increased sharply, while the lean-aged sample showed poor activity. Our results are in agreement with several other studies that reported a decrease of NH_3 oxidation after hydrothermal aging.[14,30,31]

Fig. 5 reports NH_3 conversion of all the samples at 500 °C, where the differences were more pronounced. Since slight differences existed between the degreened samples for this reaction, the conversion of individual degreened samples was reported to better assess the effect of aging. It appeared that, unlike for the standard SCR activity, there was no clear trends for the rich and lean aging. On the contrary, the catalysts aged in cycling conditions showed less deactivation than the lean- and rich-aged catalysts. This result was emphasized by the 32 h aged samples which showed less deactivation than the lean-aged sample despite the much longer net exposure to lean conditions. Alternating between rich and lean conditions therefore slowed down the deactivation for NH_3 oxidation, after exposure to 800 °C.

NH_3 storage

The storage capacity of Cu/SSZ-13 was measured before and after aging by the temperature-programmed desorption (TPD) method after NH_3 saturation at 200 °C in the presence of 5% H_2O. The results were reproducible for all degreened samples and similar desorption profiles were recorded whether TPD was performed in a bench reactor or as part of the calorimetric measurement. The results presented in Fig. 6 were obtained on a bench reactor equipped with a gas FTIR detector. For the sake of clarity, only one representative profile was plotted for the degreened catalyst. Two main features could be observed in the degreened profile: a peak centered at 400 °C and a shoulder near 295 °C, which revealed acid sites of two different strength. Above 200 °C, two types of adsorbed NH_3 species assigned to weak and strong acid sites have been frequently reported.[7,12,18,32] The high-temperature desorption peak is generally attributed to NH_3 adsorbed on Brønsted sites, while the low-temperature feature corresponds to NH_3 adsorbed molecularly on Lewis acid sites.[7,16,18,24] However, also part of the high-temperature

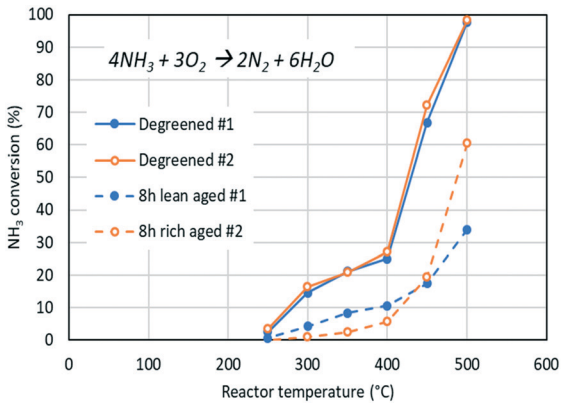

Fig. 4 NH_3 oxidation activity of degreened and aged Cu/SSZ-13 catalysts. Lean and rich-aged catalysts at all temperatures (500 ppm NH_3, 8% O_2, 5% H_2O in Ar. Total flow = 3.5 L min^{-1}). Aging at 800 °C using lean conditions (#1): 500 ppm NO, 8% O_2, 10% H_2O and 10% CO_2 and rich conditions (#2): 500 ppm NO, 1% H_2, 10% H_2O and 10% CO_2.

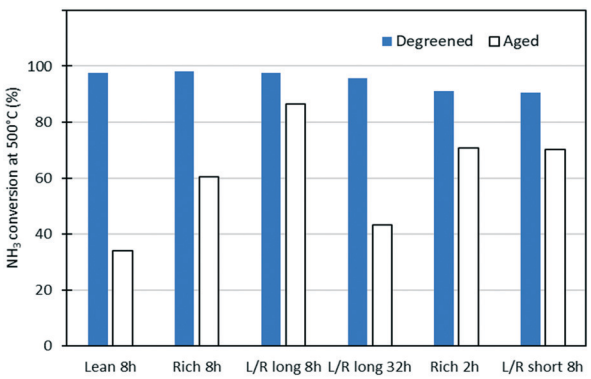

Fig. 5 NH_3 oxidation activity of degreened and aged Cu/SSZ-13 catalysts. All catalysts at 500 °C (500 ppm NH_3, 8% O_2, 5% H_2O in Ar. Total flow = 3.5 L min^{-1}). Aging at 800 °C using lean conditions: 500 ppm NO, 8% O_2, 10% H_2O and 10% CO_2 and rich conditions: 500 ppm NO, 1% H_2, 10% H_2O and 10% CO_2.

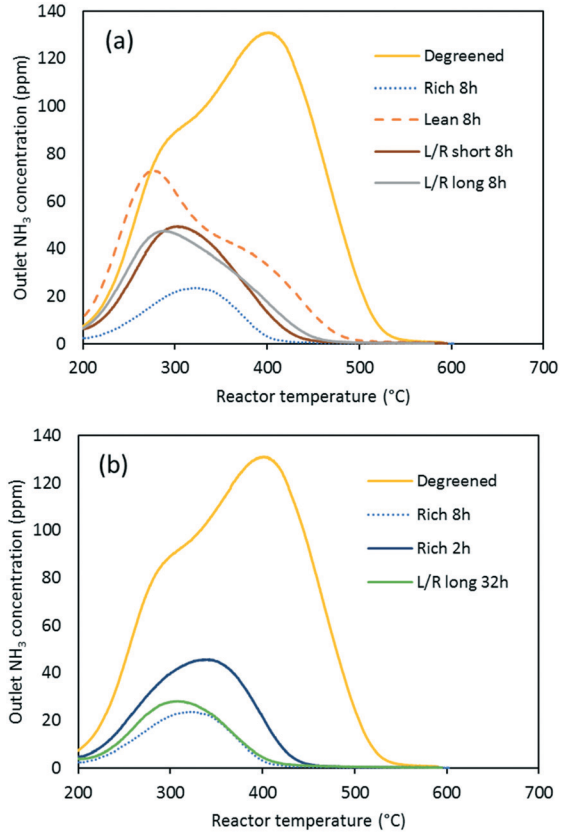

Fig. 6 NH_3-TPD of degreened and aged Cu/SSZ-13 catalysts after NH_3 saturation at 200 °C (500 ppm NH_3, 5% H_2O in Ar). Ramping from 200 °C to 600 °C (10 °C min^{-1}) (a) comparison among degreened, rich, lean and lean/rich aged catalysts (8 h at 800 °C) (b) comparison among degreened, 8 h rich, 2 h rich and 32 h lean/rich aged catalysts (800 °C). Aging was done using lean conditions: 500 ppm NO, 8% O_2, 10% H_2O and 10% CO_2 and rich conditions: 500 ppm NO, 1% H_2, 10% H_2O and 10% CO_2.

desorption peak originated from ammonia stored on copper, since this peak increased when adding copper to SSZ-13.[33]

All types of aging led to a strong decrease in total NH_3 storage, as reported in Table 2, but there was a contrast between rich (500 ppm NO, 1% H_2, 10% H_2O and 10% CO_2) and lean (500 ppm NO, 1% O_2, 10% H_2O and 10% CO_2) aging. Rich conditions caused more drastic NH_3 storage loss than lean conditions, since the storage was significantly lower after 2 h rich aging than after 8 h lean aging. Likewise, the measured storage after 8 h rich aging was lower than after 32 h lean/rich aging (Fig. 6b). Aging affected mostly the high-temperature NH_3 desorption, corresponding to Brønsted acid sites, as well as the strongly bound ammonia on the copper sites. In fact, after 8 h lean aging, the most prominent NH_3 release took place at 280 °C, showing the moderate decrease of low-temperature storage under lean conditions. These sites, assigned to the Lewis acidity, likely correspond to exchanged Cu^{2+}. The results indicated, therefore, a strong loss of available Cu after rich aging and a rather insensitivity of these sites to lean aging. The NH_3-TPD results correlate with the SCR activity measurements showing a greater impact of rich aging than lean aging. A shift towards a lower desorption temperature could also be noted after lean aging, which depicted the weakening of the remaining Lewis sites after the destruction of most of the Brønsted acid sites. In contrast, the small and broad peak obtained after rich aging (2 h and 8 h) was centred at higher temperature than the low temperature peak displayed by the fresh catalysts.

Table 2 NH_3 storage of fresh and aged catalysts measured by NH_3-TPD

Sample	NH_3 storage (μmol g^{-1})
Degreened	500
Lean 8 h	232
Rich 8 h	58
L/R long 8 h	157
L/R short 8 h	137
L/R long 32 h	72
Rich 2 h	137

NH_3 adsorption was studied at 150 °C with DRIFT spectroscopy to get more detailed information on the storage sites. The aged samples were crushed monoliths and therefore contained ≈75 wt% of cordierite, while the degreened sample was pure Cu/SSZ-13 powder, degreened under the same conditions and in the same reactor as the monolithic samples. To account for the cordierite dilution, the DRIFT spectra of the degreened sample were divided by a factor 4. The O–H stretching vibration of hydroxyl groups can be examined in Fig. 7a after NH_3 adsorption and subsequent Ar flushing (55 min). The degreened sample displayed negative bands at 3584 and 3608 cm^{-1}, which could be assigned to the Brønsted acid sites Al–OH–Si.[34–37] The bands at 3740 cm^{-1} corresponded to the terminal silanols (Si–OH) vibration.[34,35,37] The band at 3652 cm^{-1} was less clearly assigned. Aufdembrink *et al.* reported the appearance of a peak at 3650 cm^{-1} after the activation at 550 °C of an NH_4^+-exchanged chabazite zeolite.[38] They attributed this peak, with the help of ^1H NMR, to nonframework AlOH species. However, they associated a second band to these species at 3780 cm^{-1} that is absent in our spectra. Other groups assigned the band at 3650 cm^{-1} to the species $[Cu^{2+}(OH)^-]$[24,32,39] formed by coordination of a hydroxyl group to a mono-coordinated Cu cation. After lean and cycling lean/rich aging, two new bands at 3629 and 3670 cm^{-1} appeared, while the bands corresponding to Brønsted acidity were much less intense compared to the degreened spectrum. The band at 3629 cm^{-1} was assigned to the most stable Al–OH–Si. Indeed, in the SSZ-13 structure, there are four non-equivalent bridging oxygen adjacent to an Al atom, and Suzuki *et al.* demonstrated that upon aging, the most stable hydroxyl absorbing at 3622 cm^{-1} becomes predominant.[40] The band at 3670 cm^{-1} was assigned to the Al–OH groups of the extra-framework aluminum (EFAl).[41,42] Although the intensities could not directly be compared between degreened and aged samples, the relative intensity of the Brønsted sites bands and silanol bands indicated a significant loss of Brønsted sites after all three aging types. The catalyst that lost the most Brønsted acid sites was seemingly the catalyst aged in 1% H_2, in line with the NH_3-TPD results.

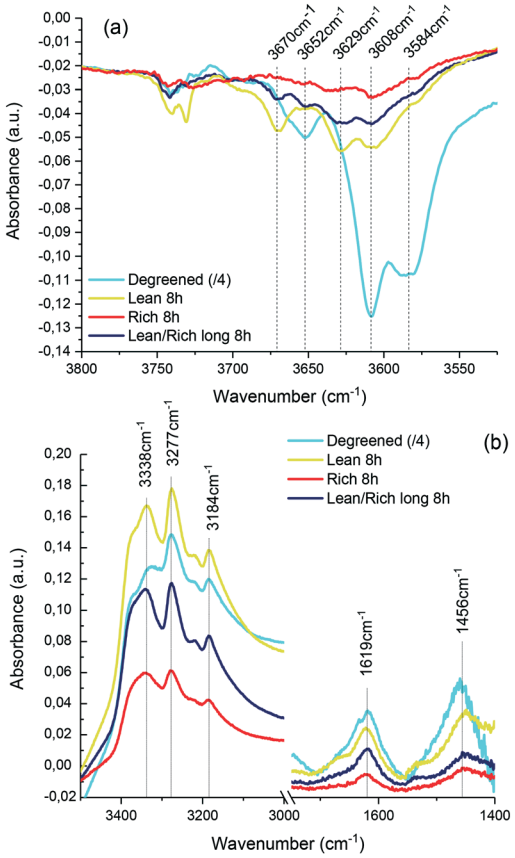

Fig. 7 DRIFT spectra recorded after 20 min NH_3 adsorption at 150 °C (1000 ppm NH_3 in Ar, total flow = 50 mL min^{-1}) and subsequent Ar flushing (55 min) on degreened, rich 8 h, lean 8 h and L/R 8 h aged samples. (a) O–H stretching region and (b) N–H stretching and bending region. The degreened catalyst absorbance was divided by 4.

Lean aging promotes the creation of EFAl species, which contribute to NH_3 storage, but these are also a sign of the dealumination process.

Fig. 7b shows the regions of N–H stretching (3000–3500 cm^{-1}) and bending (1400–1700 cm^{-1}) vibration. Ammonium ions, formed on Brønsted acid sites, and coordinated ammonia on Cu^{2+} could also be identified. The band at 1619 was associated with the bending vibration of NH_3 coordinated on Cu^{2+},[23,32,43] while the stretching vibration of these species could be noted at 3184 and 3338 cm^{-1}.[23] The bands at 3277 and 1465 cm^{-1} were assigned to the stretching and bending vibration modes of NH_4^+, respectively. The band at 3218 cm^{-1}, obscured by the bands at 3184 and 3277 cm^{-1}, could be observed in other studies of NH_3 adsorption on Cu/SSZ-13 but has not been assigned yet.[18,23,44] Fig. 7b confirms the presence of both Lewis and Brønsted NH_3 storage sites in smaller quantity after aging, especially in the rich atmosphere. Significant dealumination, which reduces NH_3 storage capacity, seems to take place during aging. Evidence of EFAl was found for lean and cycling conditions, but was not detected on the rich-aged catalyst. However, it should be noted that all bands were low in the whole region for the rich-aged sample. XRD analysis (Fig. 1) showed that the structure of the zeolite was not significantly damaged by the dealumination and that no other crystalline phase, such as Al_2O_3, was detectable. Thus, even though there was dealumination, the zeolite structure remained intact.

Finally, NH_3 adsorption and temperature-programed desorption were performed in a calorimeter on degreened and aged catalyst powder. To avoid the cordierite contribution and mass inaccuracy, the catalyst washcoat was scraped off the aged monolith for this analysis. The heat of adsorption of NH_3 at 200 °C was thus measured, and the results are presented in Fig. 8. The heat flow recorded during NH_3 adsorption was positive, which corresponded to an exothermic process. Quickly after the NH_3 flow was started, the heat flow increased to a limiting value corresponding to the heat released by the adsorption of all the fed NH_3. Later, when catalyst saturation approached and NH_3 started to slip out, the heat flow signal decreased accordingly. Fig. 8a shows the simultaneous NH_3 breakthrough and heat flow decline during NH_3 adsorption. Then, after flushing the loosely bound ammonia with argon, the temperature was ramped up and NH_3 release was observed. NH_3 desorption presented the same two peaks as detected with the monolithic sample

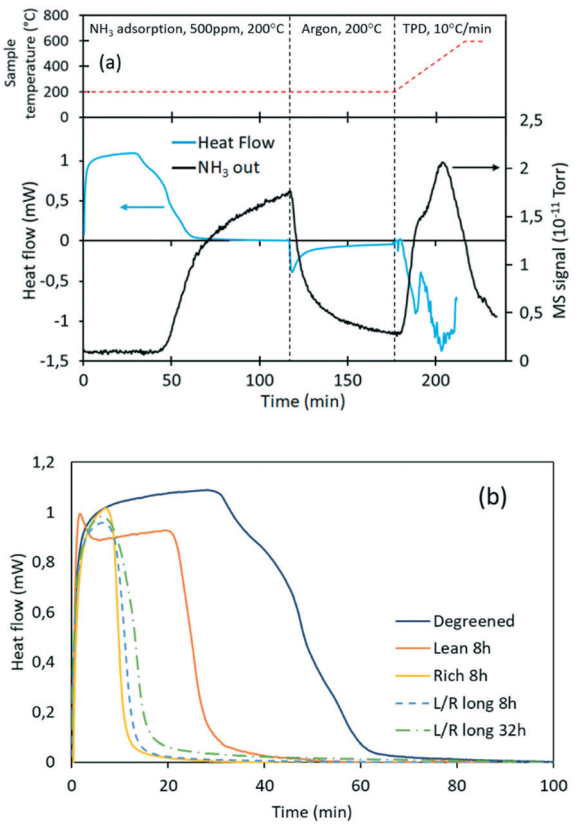

Fig. 8 (a) Calorimetric and mass spectrometry measurements (m/z = 17) during NH_3 adsorption in dry conditions at 200 °C and subsequent NH_3-TPD. (b) Comparison of the heat flow profiles obtained on degreened and aged Cu/SSZ-13 upon the introduction of 500 ppm NH_3 at t = 0. Aging at 800 °C using lean conditions: 500 ppm NO, 8% O_2, 10% H_2O and 10% CO_2 and rich conditions: 500 ppm NO, 1% H_2, 10% H_2O and 10% CO_2.

measurements. The heat flow drop corresponding to low-temperature NH_3 desorption occurred at 318 °C. The adsorption enthalpy was directly derived from the plateau level during the full NH_3 adsorption regime according to relation (1):

$$\Delta H_{ads} = -\frac{\dot{Q}}{F^{in}_{NH_3}}\frac{RT}{P} \quad (1)$$

where ΔH_{ads} is the enthalpy of adsorption of NH_3 in J mol^{-1}, $F^{in}_{NH_3}$ is the inlet volumetric flow of NH_3 in m^3 s^{-1} and $\dot{Q}$ is the measured heat flow in W.

While after rich aging the heat flow seemed to follow the heat flow profile obtained for the degreened catalyst, lean aging caused a significant decrease in NH_3 adsorption enthalpy from −158 to −136 kJ mol^{-1}. This result agrees with the TPD results that showed a shift to lower temperature for NH_3 desorption in the case of the lean-aged catalyst. Indeed, a lower enthalpy of adsorption indicates that NH_3 is less strongly bound and will desorb at lower temperature. Due to the lower storage capacity and therefore faster saturation, the measurement of the adsorption enthalpy after rich aging and L/R aging did not fully reach a plateau value, but there was a clear trend depicting the decrease in adsorption enthalpy by lean aging. NH_3 adsorption on Cu-exchanged zeolite is known to be coverage-dependent.[45,46] The average values measured in the present study are in agreement with the one reported for Cu/ZSM-5[45,47] and Cu/beta.[46] The value of −158 kJ mol^{-1} for the degreened catalyst is in agreement with −163.4 kJ mol^{-1} measured by Olsson *et al.*[29] at zero coverage.

STEM-EDX analysis

At a macroscopic level, catalysts aged in rich conditions turned purple, suggesting the presence of Cu^0,[11] while the lean-aged catalyst maintained the same typical light blue colour as the fresh catalyst, which is a sign of Cu^{2+}. The catalysts were further examined at the microscopic level by scanning transmission electronic microscopy and energy-dispersive X-ray spectroscopy. The purpose of performing these analyses was to reveal the state and location of the exchanged copper on the fresh catalyst and its evolution upon aging. Representative catalysts particles were isolated and can be seen in Fig. 9 for the fresh, the lean-aged and the rich-aged catalyst. The top row shows the HAADF image of each catalyst and the other rows are the results of EDX mapping for the elements Cu, Si and Al, from top to bottom, respectively. The fresh catalyst showed a homogeneous distribution of Cu over the studied particle, indicating a random location of aluminium sites and high Cu dispersion in the form of exchanged atomic species. Song *et al.*[31] also obtained an homogeneous composition of their Cu/SSZ-13 catalyst and, consequently, were unable to detect any Cu nanoparticles or CuO clusters. Interestingly, after rich aging at 800 °C, particles with brighter area were noticed and analyzed by EDX. As shown in Fig. 9, the brighter area corresponds to a Cu-rich particle, the

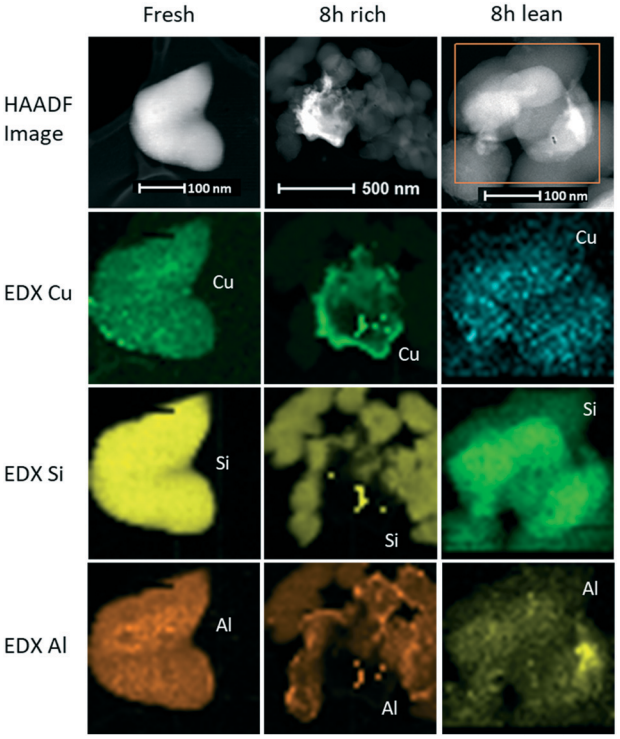

Fig. 9 STEM images and EDX elemental mapping for Cu, Si and Al of Cu/SSZ-13 before (left) and after aging 8 h in rich conditions (centre) and 8 h in lean conditions (right). Aging at 800 °C using lean conditions: 500 ppm NO, 8% O_2, 10% H_2O and 10% CO_2 and rich conditions: 500 ppm NO, 1% H_2, 10% H_2O and 10% CO_2.

size of which was over 300 nm. The constituting elements of the zeolite framework (Si, O and Al) were not observed on the bright area. Interestingly, Cu was not detected in the catalyst around the bright particle, whereas Cu was evenly spread through the whole catalyst before aging. We can conclude that the bright particles formed during rich aging were Cu particles obtained *via* the migration and agglomeration of exchanged Cu^{2+} from the surrounding catalyst. After hydrothermal aging, Song *et al.* reported the same high homogeneity of their catalyst,[31] which confirmed the specific effect of rich conditions to favour Cu migration and agglomeration outside the zeolite framework. However, in line with Song *et al.*,[31] lean aging did not lead to such Cu segregation outside the zeolite framework. As depicted in Fig. 9, Cu was still evenly dispersed over the zeolite particle. However, the distribution of Cu seemed to be less homogeneous than for the fresh catalyst. This could suggest the formation of small CuO_x clusters as a result of lean aging. This would be consistent with the NH_3 storage loss measured after lean aging, which indicates a certain loss of available Cu sites. Schmieg *et al.* demonstrated the growth of small Cu particles up to 10 nm after hydrothermal aging at 800 °C for 120 h.[14] The distribution of Al was also affected by aging. The EDX mapping of the fresh catalyst showed an even distribution of Al, whereas several spots with higher Al concentration could be noted on the outer edge of the catalyst particles after rich aging. A zone with

high Al concentration could be also readily detected after lean aging, suggesting the segregation of Al induced by both types of aging. Aluminium migration and segregation is a sign of dealumination.

Correlating the microscopy analysis with the activity results, there was an evident relationship between the Cu particle size and SCR activity. The formation of large Cu particles tremendously impairs SCR activity. The conversion of exchanged atomic Cu into small Cu clusters is significantly detrimental as well. With Cu migration and sintering being clearly accelerated by H_2 treatment, the rich conditions thus led to a rapid deterioration of the CuSSZ-13 catalyst. We propose that H_2 can reduce exchanged Cu^{2+} to Cu^0, which can then easily migrate to form large particles outside the framework without damaging the structure. The created protons bind to the aluminium to balance the charge.

Conclusions

In order to increase the operational window of NO_x reduction in diesel vehicles, LNT and NH_3 SCR can be combined. However, during deSO_x cycles of the lean NO_x-trap catalyst, the SCR catalyst can be exposed to rich conditions at high temperature. In this work, we therefore studied the aging of Cu-exchanged SSZ-13 catalysts in different conditions. The catalysts were tested and aged in various lean (500 ppm NO, 8% O_2, 10% H_2O and 10% CO_2) and rich (500 ppm NO, 1% H_2, 10% H_2O and 10% CO_2) conditions at 800 °C to simulate the conditions of deSO_x cycles of a lean NO_x-trap catalyst. The results after aging revealed an activity loss for all catalysts as well as a loss of acid sites. However, the effect of rich exposure in H_2 was extremely powerful and led to very low NO and NH_3 conversion over the whole temperature window studied (125–500 °C). Lean aging caused only a significant activity loss below 250 °C. Interestingly, aging in cycling conditions for 32 h (30 h lean and 2 h rich) resulted in the same low temperature activity as aging in 2 h rich conditions only. These results show that adding lean events in between the rich phases does not hinder or reverse the deactivation; rather, it is the time in rich conditions that determines the extent of the deactivation. STEM and EDX analysis evidenced the formation of large Cu particle by the migration of exchanged Cu atoms outside the zeolite framework during rich aging, whereas Cu remained evenly dispersed in the zeolite during lean aging. We propose that the rapid deactivation during rich aging is due to the promotion of Cu migration and agglomeration in the presence of hydrogen. Moreover, dealumination was also enhanced in rich aging. Our results show the importance of considering that the SCR system can potentially be exposed to other gases when combined with an LNT catalyst. Future studies examining a production-oriented LNT component and rich conditions from a real engine would be very interesting.

Conflicts of interest

There are no conflicts to declare.

Acknowledgements

We would like to acknowledge the funding from REWARD: REal World Advanced Technologies foR Diesel Engines project. This project has received funding from the European Union's Horizon 2020 research and innovation programme under grant agreement No 636380. We would also like to thank Swedish Energy agency (FFI, 44009-41) for the funding.

Notes and references

1 C. Courson, A. Khalfi, H. Mahzoul, S. Hodjati, N. Moral, A. Kiennemann and P. Gilot, *Catal. Commun.*, 2002, **3**, 471–477.
2 U. De La Torre, M. Urrutxua, B. Pereda-Ayo and J. R. González-Velasco, *Catal. Today*, 2016, **273**, 72–82.
3 Y. Liu, M. P. Harold and D. Luss, *Appl. Catal., B*, 2012, **121–122**, 239–251.
4 Y. Liu, Y. Zheng, M. P. Harold and D. Luss, *Appl. Catal., B*, 2013, **132–133**, 293–303.
5 J. Wang, Y. Ji, G. Jacobs, S. Jones, D. J. Kim and M. Crocker, *Appl. Catal., B*, 2014, **148–149**, 51–61.
6 L. Xu and R. W. McCabe, *Catal. Today*, 2012, **184**, 83–94.
7 U. De-La-Torre, B. Pereda-Ayo, M. Moliner, J. R. González-Velasco and A. Corma, *Appl. Catal., B*, 2016, **187**, 419–427.
8 L. Xu, R. McCabe, W. Ruona and G. Cavataio, *SAE Tech. Pap. Ser.*, 2009, 9-2009-01-0285.
9 Y. Huang, Y. Cheng and C. Lambert, *SAE Int. J. Fuels Lubr.*, 2008, **1**, 466–470.
10 Y. J. Kim, J. K. Lee, K. M. Min, S. B. Hong, I.-S. Nam and B. K. Cho, *J. Catal.*, 2014, **311**, 447–457.
11 J. H. Kwak, D. Tran, S. D. Burton, J. Szanyi, J. H. Lee and C. H. F. Peden, *J. Catal.*, 2012, **287**, 203–209.
12 K. Leistner, A. Kumar, K. Kamasamudram and L. Olsson, *Catal. Today*, 2018, **307**, 55–64.
13 Supriyanto, A. Kumar, S. Joshi, K. Kamasamudram, N. W. Currier, A. Yezerets and L. Olsson, *Appl. Catal., B*, 2015, **163**, 382–392.
14 S. J. Schmieg, S. H. Oh, C. H. Kim, D. B. Brown, J. H. Lee, C. H. F. Peden and D. H. Kim, *Catal. Today*, 2012, **184**, 252–261.
15 P. G. Blakeman, E. M. Burkholder, H. Y. Chen, J. E. Collier, J. M. Fedeyko, H. Jobson and R. R. Rajaram, *Catal. Today*, 2014, **231**, 56–63.
16 D. Wang, Y. Jangjou, Y. Liu, M. K. Sharma, J. Luo, J. Li, K. Kamasamudram and W. S. Epling, *Appl. Catal., B*, 2015, **165**, 438–445.
17 D. W. Brookshear, J. G. Nam, K. Nguyen, T. J. Toops and A. Binder, *Catal. Today*, 2015, **258**, 359–366.
18 Y. Shan, X. Shi, Z. Yan, J. Liu, Y. Yu and H. He, *Catal. Today*, 2019, **320**, 84–90.
19 K. Wijayanti, S. Andonova, A. Kumar, J. Li, K. Kamasamudram, N. W. Currier, A. Yezerets and L. Olsson, *Appl. Catal., B*, 2015, **166–167**, 568–579.
20 D. W. Fickel, E. D'Addio, J. A. Lauterbach and R. F. Lobo, *Appl. Catal., B*, 2011, **102**, 441–448.
21 W. Su, Z. Li, Y. Peng and J. Li, *Phys. Chem. Chem. Phys.*, 2015, **17**, 29142–29149.

22 C. Fan, Z. Chen, L. Pang, S. Ming, X. Zhang, K. B. Albert, P. Liu, H. Chen and T. Li, *Appl. Catal., A*, 2018, **550**, 256–265.
23 S. Han, J. Cheng, C. Zheng, Q. Ye, S. Cheng, T. Kang and H. Dai, *Appl. Surf. Sci.*, 2017, **419**, 382–392.
24 F. Gao, N. M. Washton, Y. Wang, M. Kollár, J. Szanyi and C. H. F. Peden, *J. Catal.*, 2015, **331**, 25–38.
25 S. I. Zones, *J. Chem. Soc., Faraday Trans.*, 1991, **87**, 3709–3716.
26 K. Leistner, O. Mihai, K. Wijayanti, A. Kumar, K. Kamasamudram, N. W. Currier, A. Yezerets and L. Olsson, *Catal. Today*, 2015, **258**, 49–55.
27 L. Ma, Y. Cheng, G. Cavataio, R. W. McCabe, L. Fu and J. Li, *Appl. Catal., B*, 2014, **156–157**, 428–437.
28 C. Paolucci, I. Khurana, A. A. Parekh, S. Li, A. J. Shih, H. Li, J. R. Di Iorio, J. D. Albarracin-Caballero, A. Yezerets, J. T. Miller, W. N. Delgass, F. H. Ribeiro, W. F. Schneider and R. Gounder, *Science*, 2017, **357**, 898–903.
29 L. Olsson, K. Wijayanti, K. Leistner, A. Kumar, S. Y. Joshi, K. Kamasamudram, N. W. Currier and A. Yezerets, *Appl. Catal., B*, 2015, **174–175**, 212–224.
30 J. Luo, D. Wang, A. Kumar, J. Li, K. Kamasamudram, N. Currier and A. Yezerets, *Catal. Today*, 2016, **267**, 3–9.
31 J. Song, Y. Wang, E. D. Walter, N. M. Washton, D. Mei, L. Kovarik, M. H. Engelhard, S. Prodinger, Y. Wang, C. H. F. Peden and F. Gao, *ACS Catal.*, 2017, **7**, 8214–8227.
32 I. Lezcano-Gonzalez, U. Deka, B. Arstad, A. Van Yperen-De Deyne, K. Hemelsoet, M. Waroquier, V. Van Speybroeck, B. M. Weckhuysen and A. M. Beale, *Phys. Chem. Chem. Phys.*, 2014, **16**, 1639–1650.
33 K. Leistner, K. Xie, A. Kumar, K. Kamasamudram and L. Olsson, *Catal. Lett.*, 2017, **147**, 1882–1890.
34 F. Ayari, M. Mhamdi, D. P. Debecker, E. M. Gaigneaux, J. Alvarez-Rodriguez, A. Guerrero-Ruiz, G. Delahay and A. Ghorbel, *J. Mol. Catal. A: Chem.*, 2011, **339**, 8–16.
35 P. Bräuer, P. L. Ng, O. Situmorang, I. Hitchcock and C. D'Agostino, *RSC Adv.*, 2017, **7**, 52604–52613.
36 V. B. Kazansky, A. I. Serykh, V. Semmer-Herledan and J. Fraissard, *Phys. Chem. Chem. Phys.*, 2003, **5**, 966–969.
37 G. L. Woolery, L. B. Alemany, R. M. Dessau and A. W. Chester, *Zeolites*, 1986, **6**, 14–16.
38 B. A. Aufdembrink, D. P. Dee, P. L. McDaniel, T. Mebrahtu and T. L. Slager, *J. Phys. Chem. B*, 2003, **107**, 10025–10031.
39 F. Giordanino, P. N. R. Vennestrøm, L. F. Lundegaard, F. N. Stappen, S. Mossin, P. Beato, S. Bordiga and C. Lamberti, *Dalton Trans.*, 2013, **42**, 12741–12761.
40 K. Suzuki, G. Sastre, N. Katada and M. Niwa, *Phys. Chem. Chem. Phys.*, 2007, **9**, 5980–5987.
41 A. A. Gabrienko, I. G. Danilova, S. S. Arzumanov, L. V. Pirutko, D. Freude and A. G. Stepanov, *J. Phys. Chem. C*, 2018, **122**, 25386–25395.
42 F. Benaliouche, Y. Boucheffa, P. Ayrault, S. Mignard and P. Magnoux, *Microporous Mesoporous Mater.*, 2008, **111**, 80–88.
43 J. Luo, F. Gao, K. Kamasamudram, N. Currier, C. H. F. Peden and A. Yezerets, *J. Catal.*, 2017, **348**, 291–299.
44 H. Zhu, J. H. Kwak, C. H. F. Peden and J. Szanyi, *Catal. Today*, 2013, **205**, 16–23.
45 V. Bolis, S. Bordiga, G. T. Palomino, A. Zecchina and C. Lamberti, *Thermochim. Acta*, 2001, **379**, 131–145.
46 N. Wilken, K. Kamasamudram, N. W. Currier, J. Li, A. Yezerets and L. Olsson, *Catal. Today*, 2010, **151**, 237–243.
47 V. Rakić, V. Dondur, S. Gajinov and A. Auroux, *Thermochim. Acta*, 2004, **420**, 51–57.

